A&A 375, 434–446 (2001)
DOI: 10.1051/0004-6361:20010837

Astronomy & Astrophysics

V505 Mon – An early-type binary with a disk⋆

P. Mayer[1], D. Chochol[2], H. Drechsel[3], R. Lorenz[3], M. Plavec[4], T. Raja[1], and A. H. Batten[5]

[1] Astronomical Institute of the Charles University, V Holešovičkách 2, 180 00 Praha 8, Czech Republic
[2] Astronomical Institute of the Slovak Academy of Sciences, 09 056 Tatranská Lomnica, Slovakia
[3] Dr. Remeis-Sternwarte, Astronomisches Institut der Universität Erlangen-Nürnberg, Sternwartstraße 7, 96049 Bamberg, Germany
[4] Department of Astronomy, University of California, Los Angeles, California 90025 1562, USA
[5] Dominion Astrophysical Observatory, 5071 W. Saanich Road, Victoria, B.C., V8X4M6 Canada

Received 10 April 2001 / Accepted 7 June 2001

Abstract. New spectra of the eclipsing binary V505 Mon (usually classified as B5 Ib) were obtained in the optical and UV regions. Only spectral lines of one component are visible, with $K = 93$ km s^{-1}. According to arguments based on the extent of the disk the mass ratio might be about 0.30. The star with the visible spectral lines would then have a mass of 2.3, the other component of 7.7 $M_{\odot}$, i.e. their supergiant nature can be ruled out. The distance to the system appears to be about 1 kpc. Together with published photometric data, the spectroscopy provides clear evidence for the presence of a disk around the secondary component. The profiles of the C II 1335/6 doublet lines are used to derive the rotational velocity of the disk. The structure of the disk can be characterized by a central ionized zone surrounded by neutral outer parts. Additional matter of cloudy nature has to be present, and both components are embedded in an extended atmosphere. Abundance of carbon was found to be very low. Similarity with some other non-eclipsing binaries is discussed.

Key words. binaries: eclipsing – stars: early-type – stars: individual: (V505 Mon)

1. Introduction

With its period, spectral type and Hα emission, the star V505 Mon (HD 48914) belongs to a group of binaries, for which the stellar parameters and evolutionary state are not yet well understood. Even its classification is difficult: it is not a W Ser star, due to lack of emission in the IUE UV range, nor a long-period Algol system (both components are of early type, and – as we will show below – neither component fills its Roche lobe), nor a typical Be star, since its spectral appearance is different and its rotational velocity is only modest. Finally, the strange shape of its eclipse minima makes V505 Mon a really unique case. We will, however, mention the similarity with several comparable, albeit non-eclipsing systems.

The star was found as a radial velocity variable by Pearce & Petrie (1951) and as a photometric variable by Wachmann (1966). Its brightness at maximum is $V = 7.2$. A spectral type of B5 Ib was given by Hoag & van Smith (1959), while other classifications range between B2 and B8, and luminosity classes are from III to Ib. Initially, two possible values of the period – $26\overset{\mathrm{d}}{.}95$ or $53\overset{\mathrm{d}}{.}78$ – were considered by Chochol & Kučera (1981); the longer value was later confirmed by the spectroscopic study of Stagni et al. (1982). These authors analyzed low dispersion spectra, and the detection of secondary lines was claimed. If these were real, the binary would be one of the most massive systems known. On the other hand Batten et al. (1989) noted that the secondary spectrum was actually invisible in high dispersion spectra taken at Dominion Astrophysical Observatory, Victoria, BC.

Eggen (1978) published *uvby* measurements of V505 Mon, and Chochol et al. (1985) presented UBV photometry. The star was included in the Long-Term Photometry of Variables program (Manfroid et al. 1991; 1994; Sterken et al. 1993, 1995[1]). Preliminary results of this *uvby* photometry were published by Vogt & Sterken (1993). V505 Mon is referenced in the HIPPARCOS catalogue (ESA 1997), with a parallax of 1.11 ± 0.88 mas and 105 photometric data entries. It is not contained in the IRAS catalogue (ESA 1986).

In this paper, we present new high-dispersion spectra obtained at several observatories. A total of 19 high and

Send offprint requests to: P. Mayer,
e-mail: mayer@mbox.cesnet.cz

⋆ Based on observations collected at the European Southern Observatory, La Silla, Chile, and at the German-Spanish Observatory, Calar Alto, Spain.

[1] Note that in the LTPV materials, V505 Mon is listed under an incorrect HD number 49014.

low dispersion SWP and LWP IUE spectra were also obtained. The optical and UV spectroscopy is analyzed and discussed in combination with the photometric data. We believe there has to be a two-component (neutral and ionized) disk around the secondary component; only such a disk, together with other forms of inter- and circumbinary matter, can explain various photometric or spectroscopic peculiarities. Our estimate of the mass ratio is based on the fractional size of the disk.

The photometric and optical and UV spectroscopic observations are analyzed in Sects. 2, 3 and 4. Physical parameters of the stellar components and of the circumstellar matter as well as attempt to evaluate the basic characteristics of data are presented in Sect. 5.

2. Photometry

2.1. The uvby photometry

Vogt & Sterken (1993) noted: " ... there is a strong variability in the shape of the primary eclipse minima, especially in their width, and there are also some irregular variations during the phases outside eclipses. In y, b and v, the depths of primary and secondary eclipses are nearly the same, while primary eclipses normally last longer... However, in the u band, the primary eclipses are much deeper than the secondary eclipses ...". The corresponding light curves as obtained in the LTPV program are shown in Fig. 1. The data are from 395 nights, and they consist mostly of one measurement per night (in seven cases, two measurements per night). For the calculation of orbital phases the ephemeris

$$\text{Prim. Min.} = \text{JD}2445253.71 + 53\overset{\text{d}}{.}7745 \cdot \text{E}$$

according to Vogt & Sterken was used. The primary minimum corresponds to the eclipse of the star with prominent spectral lines, which follow a radial velocity curve with a semiamplitude of about 93 $\text{km}\,\text{s}^{-1}$. We will refer to this star as the primary component. Spectral lines of the other component are invisible.

Both minima are several tenths of magnitude deep. The secondary minimum is exactly centered on phase 0.5; hence a circular orbit can be assumed, and is also supported by the symmetric shape of the radial velocity curve. The light curve is affected by a considerable scatter of about $\pm 0\overset{\text{m}}{.}06$ in vby and $\pm 0\overset{\text{m}}{.}10$ in u (note that the u magnitude scatter would be somewhat smaller if the magnitudes would be corrected for the long-period variation described in Sect. 2.3). The colour indices do not vary much with phase, only c_1 behaves differently.

Table 1 contains the parameters describing the light curves. The primary minimum in the y bandpass appears to be a superposition of a shallow "trough" with wings extending about 0.08 phase units to both sides, and of a central dip ("spike") with a total width of only 0.03 phase units. The secondary minimum is very sharp, with a width equalling that of the primary minimum spike. In the u passband the trough is much broader and double-peaked, reaching its maximum depth at phases 0.96 and 0.04, while the secondary minimum is less pronounced. The schematic representation of the y and c_1 light curves corresponding to values given in Table 1 is drawn in Fig. 1.

Table 1. Parameters of the light curves.

Colour	Maximum	Prim. min. depth		Sec. min.
		spike	*trough*	depth
y, V	7.22	0.36	0.18[a]	0.32
c_1	0.38	0.20	0.37	−0.13[b]
$B-V$	0.00	0.00	0.00	0.00
$U-B$	−0.44	0.01	0.17	−0.08[b]
u	7.79	0.54	0.50	0.22
U	6.78	0.37	0.27	0.24

[a] Wings extrapolated to phase 0.
[b] "Negative" amplitude, because c_1 and $U-B$ exhibit peaks instead of minima at phase 0.5.

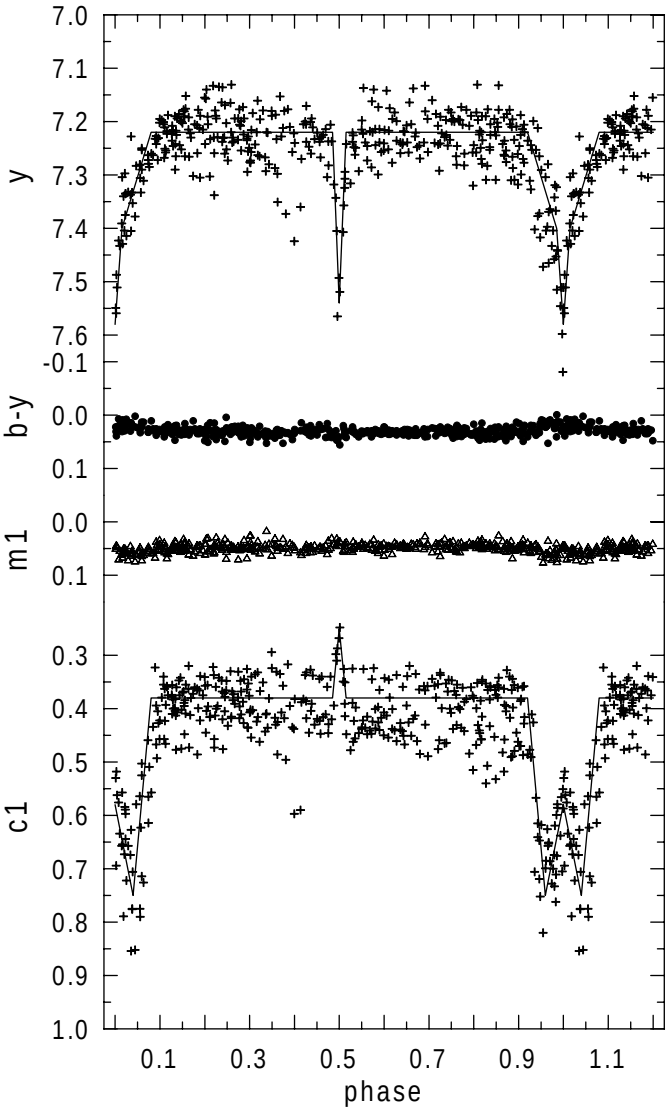

Fig. 1. LTPV data (from top to bottom: y curve; $b-y$, $m1$, $c1$).

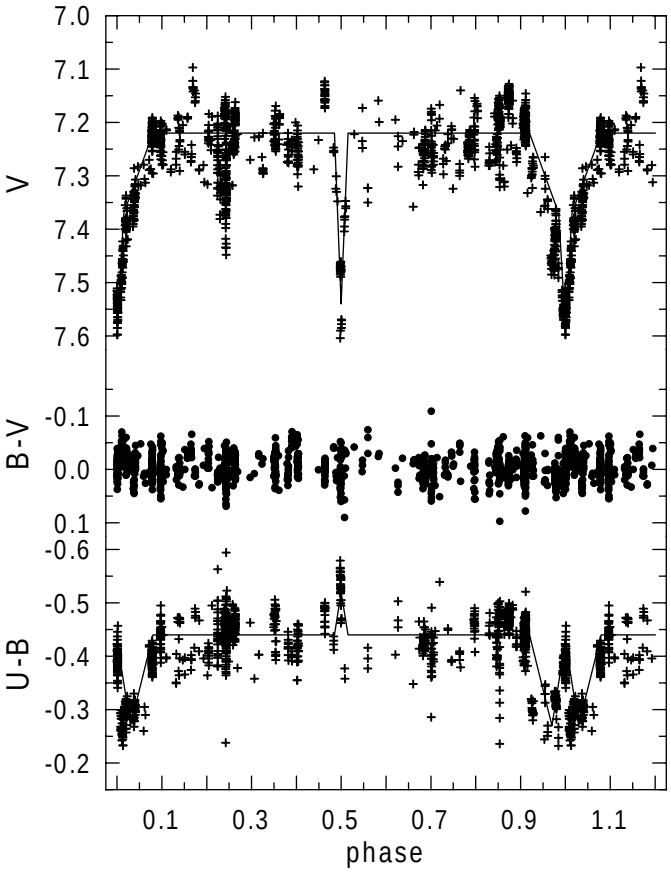

Fig. 2. UBV data (top: V, middle: $B-V$, bottom: $U-B$).

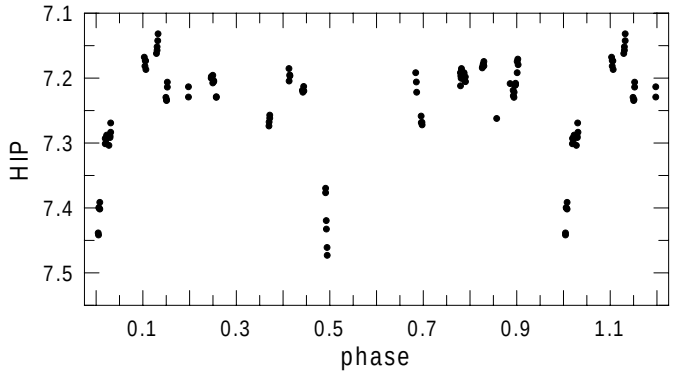

Fig. 3. HIPPARCOS photometry.

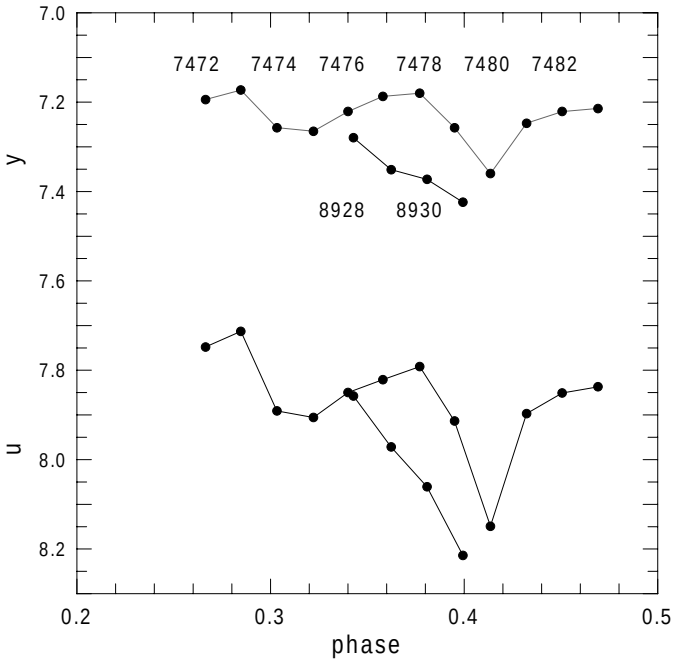

Fig. 4. Two examples of brightness drops in y (top) and u (bottom); last four digits of JD are given.

2.2. UBV and HIPPARCOS photometry

The UBV photometry obtained at several observatories was collected by one of us (DC) and presented in two papers (Chochol et al. 1985, 2001); measurements from 105 nights are given there. All observations are displayed in Fig. 2; also the schematic representation of the V and $U-B$ curves according to Table 1 is drawn. Contrary to the *uvby* data, the UBV data have a better phase resolution and consist of multiple measurements obtained during single nights.

For the $B-V$ index, no changes with phase are apparent. Changes of the $U-B$ index are similar to changes of $u-b$, however the amplitude is smaller by about 50% in the primary minimum. Already in the first paper Chochol et al. noted the presumable presence of circumstellar material in the system.

The HIPPARCOS photometry is spread over the whole phase range and includes both minima, see Fig. 3. The scatter between minima is comparable to other data. In several cases, the night series of data display quite fast changes. This effect was already recognized by Wachmann (1966) and by Chochol (1981).

2.3. Brightness variations

In *uvby* as well as in UBV photometry, considerable brightness drops were observed at out-of-minimum phases. This variability was found strongest in the UV. The deepest drops were observed in *uvby* at phase 0.40, in UBV at 0.24. Examples are given in Fig. 4.

The large scatter of brightness and colours persists also during both eclipses. The timescale of variability is much shorter than the orbital period. Our search for any periodic short-term modulations in the photometric data yielded no convincing results. However, when searching for long-period variations, a quite large modulation of u magnitude was found with a period of 3400 days, maximum attenuation at JD 2447800, and a semiamplitude of about $0\overset{\mathrm{m}}{.}055$; see Fig. 5.

In other bandpasses such long-term variations are absent – perhaps with the exception of the U band; however, the time coverage is less dense and the amplitude is smaller than in u.

Table 2. Journal of V505 Mon spectra.

Observatory	HJD-24E5	Ident.[a]	Phase	$V_{\rm rad}$[b]	$V_{\rm rad}$(Fe II)	$V_{\rm rad}$(H)[c]	Spectral coverage
DAO	45690.840		.1289	−38.7			photogr.
	45713.762		.5552	64.1			photogr.
	45725.779		.7787	118.1			photogr.
	46038.990		.6032	88.2			photogr.
	46080.823		.3811	−28.5			photogr.
	46490.625		.0019	17.8			photogr.
	46810.821		.9563	67.5			photogr.
	47951.624		.1709	−60.7			photogr.
	47977.673		.655	113.5			photogr.
	48254.897	CCD	.8106	112.7			
	48297.716	RETICON	.6069	89.9			
	48297.733	RETICON	.6072	89.7			
Ondřejov	43186.460	2748	.5571	67.1	−14	9	photogr.
	44574.581	3864	.3894	−33.3	6	−37	photogr.+ Hα
	44636.352	3918	.5195	36.5	4	−15	photogr.+ Hα
	45006.390	4365	.4008	−11.3	−124	−18	photogr.+ Hα
	45010.440	4370	.4761	17.7	−9	1	photogr.
	45011.449	4375	.4949	41.9	28	39	photogr.
	47974.328	5120	.5931	86.3	34	55	photogr.
	48682.302	5744	.7587	124.2	−44	−14, 122	photogr.
	48906.629	5870	.9303	65.9	146	−8, 123	photogr.
	49002.533	5921	.7138	119.9	−26	4, 108	photogr.
Rozen	44884.644	r755	.1368	−30.9		0	photogr.
Lick	46694.979	1	.8021	118.8	25	25, 123	3745-5895, gaps
	47607.737	2	.7759	126.1	54	81	3558-8677, gaps
	49382.8092	3	.7875	123.0	−12		4407-6894, gaps
	49383.7647	4	.8053	122.4	−12		4407-6894, gaps
Asiago	48910.685		.0057	37.5			5580-6780, gaps
ESO	48674.597	ECHELEC	.6154	85	−41		4600-4880
	49448.4641	CAT 1	.0064	17			4900-4940
	49449.4626	CAT 2	.0249	8			4900-4940
	49450.4674	CAT 3	.0436	−10			4900-4940
	49451.4620	CAT 4	.0622	−13			4900-4940
	49452.4587	CAT 5	.0807				6545-6580
	49453.4604	CAT 6	.0993	−32			4900-4940
	49454.4589	CAT 7	.1179	−41			4900-4940
Calar Alto	49000.514	1	.6762	113[d]			6514-6724
	49001.469	2	.6940	122		117	4822-5035
	49326.562	3	.7395	121[d]			6521-6722
	49327.703	4	.7607	125		117	4824-5034
	49330.633	5	.8152	113[d]			6515-6722

[a] Type or number of the spectrum.
[b] Radial velocities used to evaluate V_0, K_1: results from He I lines in case of DAO, Ondrejov, Rozen, Asiago and Calar Alto data, and from N II, S II lines in case of Lick and ESO data.
[c] Hα not included.
[d] He I 6678.

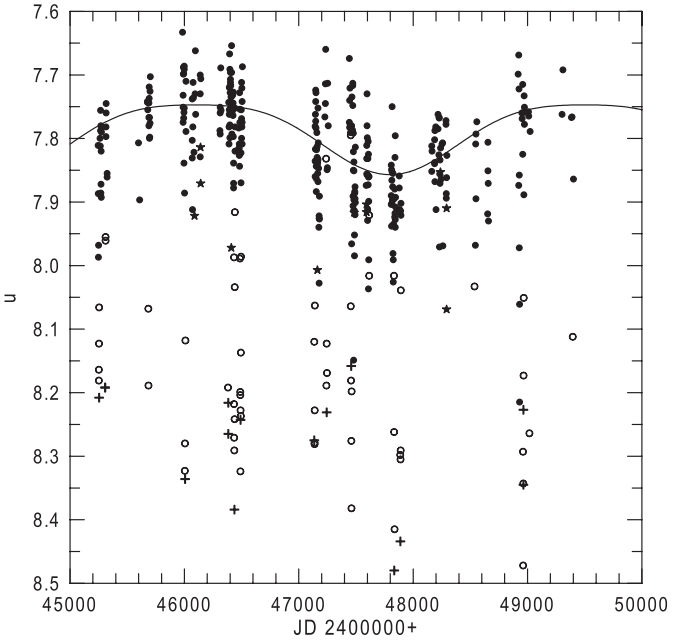

Fig. 5. Long-period variations of the u magnitude. Filled circles – measurements between minima; crosses – phase 0.985–0.015; open circles – phase 0.920–0.985 and 0.015–0.080; star symbols – phase 0.485–0.515. The fit curve corresponds to $0.055\sin(2\pi\tau) + 0.022\sin^2(2\pi\tau) + 7.78$, where $\tau = (\mathrm{JD}-2446950)/3400$.

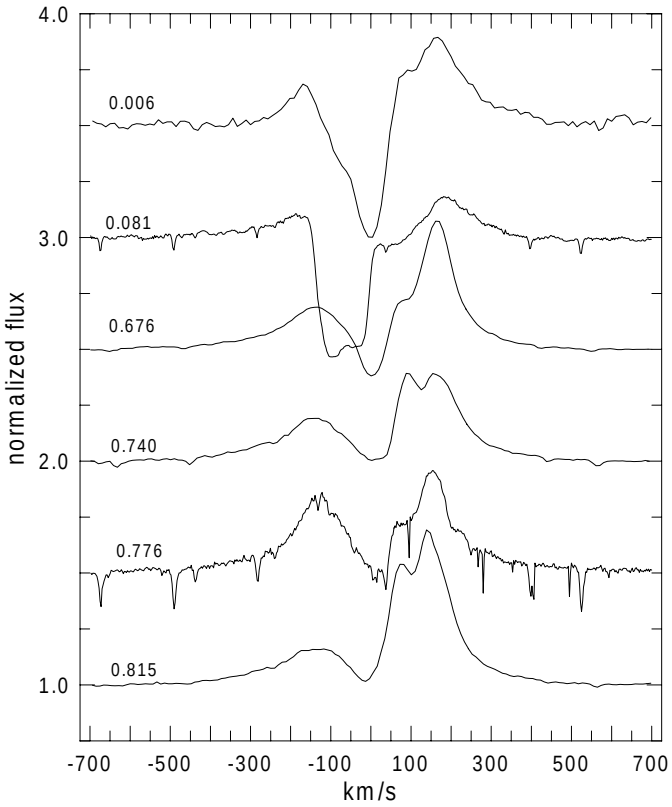

Fig. 6. Examples of profiles of the Hα line; note that at phase 0.006, the continuum level is $0\overset{\mathrm{m}}{.}3$ lower than at other phases, therefore EW of Hα is 0.76 times smaller than pretended by the graph.

3. Spectroscopy in the optical region

Our analysis is based on photographic and electronic spectra taken at various observatories. Photographic spectra were obtained at the Dominion Astrophysical Observatory (Canada) with the coudé spectrograph of the 1.2 m telescope, with a dispersion of 6.5 Å mm^{-1}; at Ondřejov (Czech Republic) with the coudé spectrograph of the 2 m telescope, with a dispersion of 17 Å mm^{-1}, and at Rožen (Bulgaria), also with the coudé spectrograph of the 2 m telescope and a dispersion of 17 Å mm^{-1}; electronic spectra were also taken at the Dominion Astrophysical Observatory with the same spectrograph mentioned above with dispersion 20 Å mm^{-1} (RETICON) and with the Cassegrain spectrograph of the 1.8 m telescope with dispersion 15 Å mm^{-1} (CCD); at Lick Observatory (USA), with the Hamilton echelle spectrograph of the 3 m telescope; at Asiago Observatory (Italy), with the echelle spectrograph of the 1.82 m telescope; at ESO La Silla (Chile), with the ECHELEC instrument of the 1.52 m ESO telescope as well as with the 1.4 m CAT and the coudé spectrograph of the ESO 3.6 m telescope; and at Calar Alto Observatory (Spain), with the coudé spectrograph of the 2.2 m telescope. For a journal of spectra see Table 2. Resolution of CCD spectra is between about 10 000 (Asiago) and 50 000 (Hamilton and CAT/CES).

The spectra obtained at Dominion Astrophysical Observatory were evaluated independently of others. Stagni et al. (1982) noted that all the old velocity measurements by Pearce & Petrie (1951) and Petrie & Pearce (1961), except the first one, are compatible with a period of $53\overset{\mathrm{d}}{.}78$. We remeasured the old plates and found good agreement with the original measurements, except again for the first one. Instead of the published value of -18.6 km s^{-1}, a value close to $+120$ km s^{-1} was derived – consistent with a period near $53\overset{\mathrm{d}}{.}8$.

For the present purpose, the old data were not used. From the new DAO spectra radial velocities were determined using lines of He I, Si II and Mg II. From these velocities we get $K_1 = 92.2$ km s^{-1} and $V_0 = +27.9$ km s^{-1}. The velocity for phase 0.956 was not taken into account, since it showed a large residual. The hydrogen lines always gave systematically smaller velocities than the other lines. Using He I 4471 and Mg II lines the rotational velocity was found as $v_{\mathrm{rot}} \sin i = 45 \pm 5$ km s^{-1}.

3.1. Description of spectral lines

The star eclipsed during the primary minimum exhibits clearly visible absorption lines of ions He I, Mg II, Si II and III, O II, N II and S II; their velocities follow a sinusoidal radial velocity curve with $K_1 = 93$ km s^{-1}. However, other line components or line profile distortions are present. Figs. 6 to 10 show some examples of spectral lines in the optical region (only electronic spectra are shown in these figures).

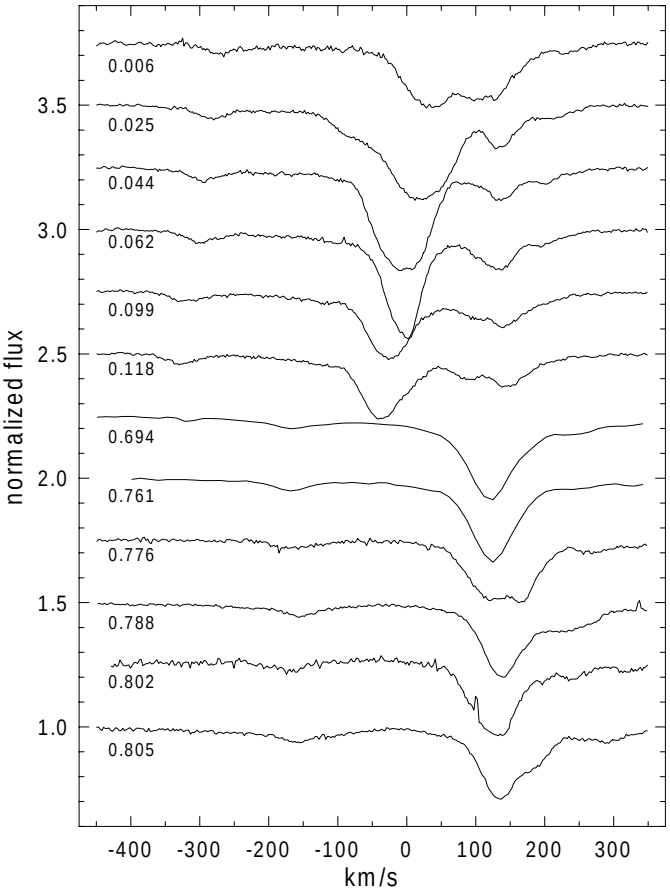

Fig. 7. Examples of profiles of the He I 4922 line; note the deep profiles at phases where the effect of the disk is expected; the line at left side is S II 4917.

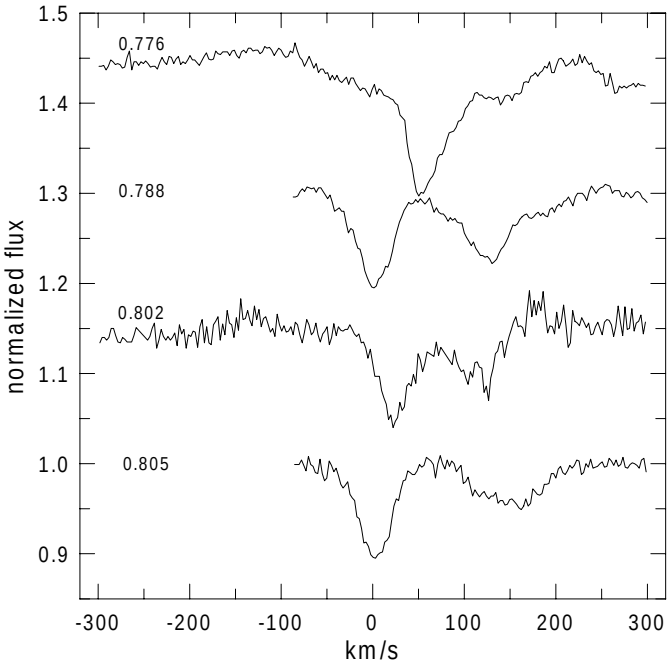

Fig. 8. Examples of profiles of the Fe II 5169 line. The line to the right is Fe I 5171.

It is obvious that various spectral lines exhibit quite different characteristics:

- Hα (Fig. 6) is the only line with an emission component. The emission profile appears to be double-peaked, i.e. a central depression divides the emission feature into red- and blue-shifted peaks. The separation of the peaks is approximately 6.7 Å, and this value fits the relation between the separation and orbital period found by Olson & Etzel (1995) for long period Algols (however note that V505 Mon is not a typical Algol). The red peak is always more prominent. Emission is present with a width of about 400 km s^{-1}, and a height of 40 to 60% above continuum level; the emission appears stationary, certainly it is not correlated with the orbital motion of the primary star. There are several absorption components; they are variable and deepest at phases near primary minimum, where the flux drops to about 50% of the continuum level. The steep borders of the absorption profile at phase 0.081 suggest that the line is saturated. Therefore the residual half of light should come from the secondary component. At other phases, the depth of the absorption only varies by 0–10% of the continuum. A component with about zero velocity is always present.

  Other Balmer lines are often split into two or more components, and similarly to Hα, the main component has zero velocity. The component with radial velocity close to the overall sinusoidal run of other lines is not always present;
- Helium lines (Fig. 7) usually have some strange components; at phase 0.930, a high velocity component is present (+280 km s^{-1}, visible in the photographic spectrum Ondřejov 5870 in lines He I 4713, 4922 and 5015). In a given spectrum, line components or distortions look differently for different lines. Note that at phases 0.025, 0.044 and 0.062, the He I 4922 line is deeper than at other phases (the equivalent widths are to be multiplied by 0.87, 0.94 and 0.97, respectively, due to the continuum variation during eclipse);
- Numerous lines are due to N II and S II. They appear less distorted than He I lines, and hence should provide the most reliable orbital velocities;
- Many weak lines belong to Fe II (Fig. 8). The corresponding velocities differ from the orbital velocity and do not depend on phase. E.g. in Lick spectra 1 and 2 taken at nearly identical phases they have different velocities: +25 km s^{-1} at phase 0.802, and +54 km s^{-1} at phase 0.776. In Lick spectra 3 and 4, one component has velocity −12 km s^{-1} in both spectra, while the velocities of the other components strongly deviate: +112 or 138 km s^{-1}. Velocities very different from the orbital velocity are also found in photographic spectra;
- The Na D lines (Fig. 9) only appear as sharp interstellar components at phases around 0.75; at phase 0.006, the lines spread out to about −100 km s^{-1}. In Ca II lines, a component with a velocity close to the sinusoidal curve is discernible in several spectra, besides an interstellar component. However, at phase 0.930,

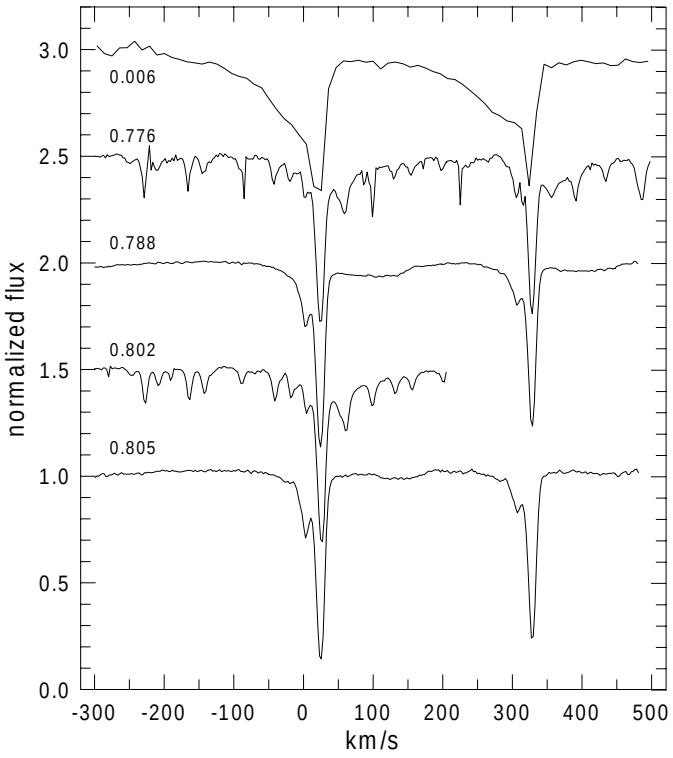

Fig. 9. Examples of profiles of the Na D line; the spectrum at phase 0.006 is of lower resolution; the spectra at phases 0.788 and 0.805 are by Dr. Popper and have been divided by a spectrum of an A type star in order to suppress the terrestrial lines.

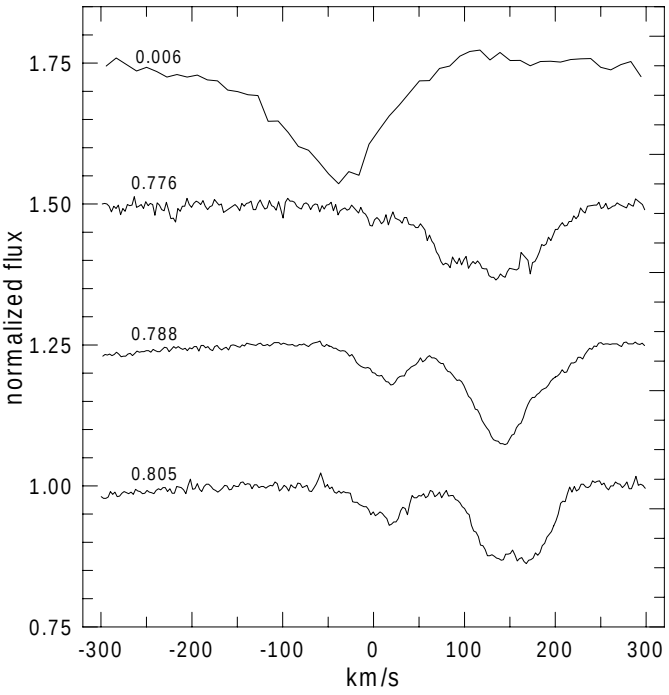

Fig. 10. Examples of profiles of the Si II 6347 line.

the velocity does not agree with the radial velocity curve and equals that of Balmer lines;

– The line Si II 6347 (Fig. 10) is covered by three CCD spectra around phase 0.75 (Fig. 10). In two cases, besides the primary component line, also a component with velocity +5 km s^{-1} is present. This velocity differs from the velocities of Fe II lines. The extension of its blue wing in the spectrum taken at phase 0.006 is similar as in the Na D lines;

The radial velocities are displayed in Fig. 11. The semi-amplitude and the systemic velocity as calculated from values in the column "$V_{\rm rad}$" of Table 2 amount to $K_1 = 93.4$ and $V_0 = +28.3$ km s^{-1}. A value of $a_1 \sin i = 99\ R_\odot$ is derived, and the mass function is $f(m_2) = 4.55\ M_\odot$.

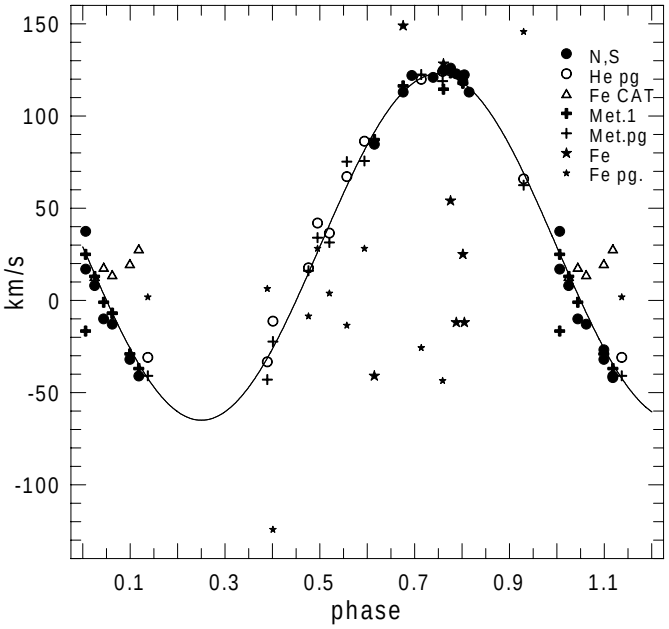

Fig. 11. Radial velocities measured in V505 Mon spectra; the solid line corresponds to orbital elements given in Sect. 3.1.

4. IUE spectra

4.1. The continuum

A list of IUE spectra of V505 Mon is given in Table 3. The 1996 spectra were obtained according to an application by the present authors HD, RL, MP and PM. We intended to obtain more spectra under this program, but the satellite life ended before all planned exposures could be finished.

To find the best fit of observed and theoretical spectra, low dispersion IUE spectra are usually used. In this case, however, the available spectra are rather noisy, so we used high dispersion spectra and averaged the data by binning at the wavelength grid points used by Kurucz (1993). Even then, namely the long wavelength spectra were still noisy. Nevertheless, according to Fig. 12, one can judge that the applied correction for interstellar extinction – $E_{B-V} = 0.10$ – is conceivably right, and $T_{\rm eff} = 15\,000$ K represents a good fit, perhaps with a $\log g$ value smaller than that of a main sequence star. The long wavelength spectrum (i.e. $\lambda > 1970$ Å) at phase 0.064 is probably affected by the disk.

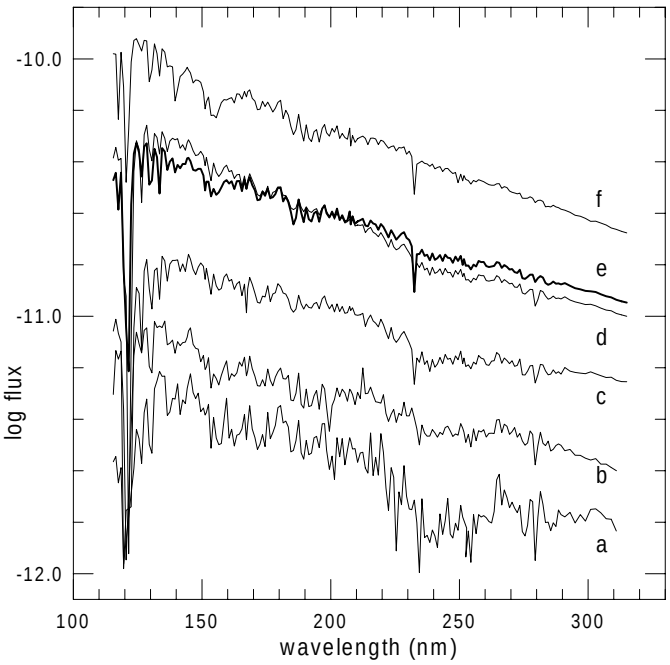

Fig. 12. Observed and theoretical spectra: **a)** spectrum at phase 0.066; **b)** spectrum at phase 0.164; models: **c)** $T_{\rm eff}$ = 13 000 K, $\log g$ = 2.5; **d)** $T_{\rm eff}$ = 15 000 K, $\log g$ = 2.5; **e)** $T_{\rm eff}$ = 15 000 K, $\log g$ = 4.5 (thick line); **f)** $T_{\rm eff}$ = 18 000 K, $\log g$ = 2.5.

Table 3. The IUE spectra.

Camera	HJD-24E5	Exposure	Resolution	Phase
SWP	45645.768	21465	high	0.292
	45746.648	22276	high	0.169
	47623.238	35949	low	0.064
	47623.272	35950	high	0.065
	47626.251	35969	high	0.121
	47626.338	35970	low	0.122
	50133.736	56835	low	0.750
	50133.783	56836	high	0.751
	50142.133	56864	high	0.906
	50142.186	56865	low	0.907
	50143.654	56870	high	0.934
	50145.236	56881	high	0.964
	50147.639	56892	low	0.008
LWP	45645.759	02238	low	0.291
	45746.679	02787	high	0.167
	47623.242	15314	low	0.064
	47623.320	15315	high	0.066
	47626.298	15330	high	0.121
	47626.342	15331	low	0.122

4.2. The spectral lines

The UV line spectrum of V505 Mon contains numerous lines of stellar, circumstellar and interstellar origin. Some lines have complex profiles, because they are formed as blends of different components. As an example, the resonance doublet of C II 1335/6 is shown in Fig. 13. Several features can be recognized:

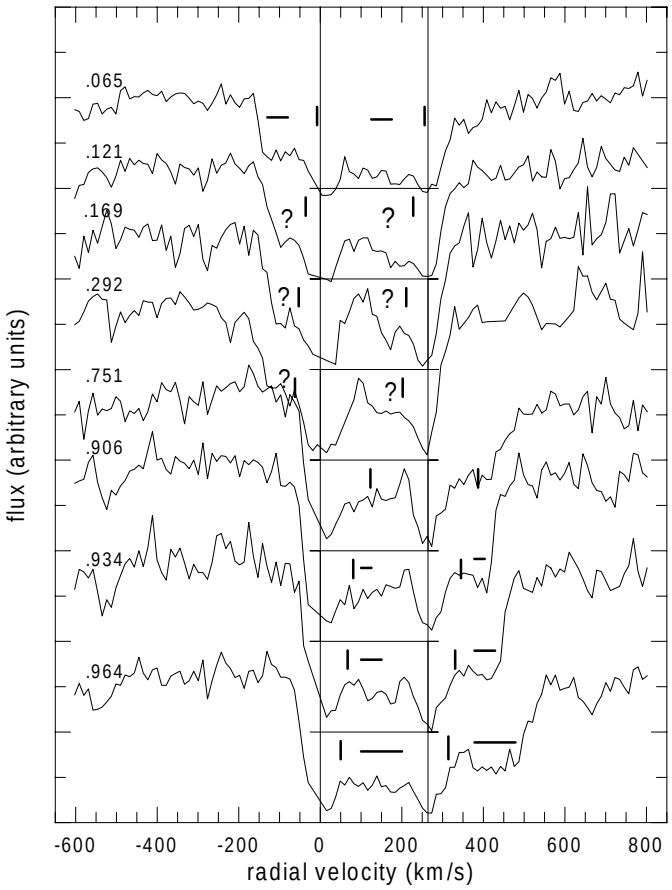

Fig. 13. Profiles of the C II 1335/6 doublet. The vertical lines correspond to zero velocity of both spectral lines, horizontal lines define zero intensity of the profiles. The short vertical bars mark the expected primary component orbital velocity, the thick horizontal lines mark the disk contribution. For features marked "?" see text.

- The deepest, wide component with velocity close to zero must originate in a common binary envelope (as is also true for respective components in the Hα profile and in other lines). It cannot be interstellar, since the main interstellar contribution, according to the Na D profile, is much narrower. To be sure about the origin of these wide structures, we checked also lines listed by Stickland (1987) as interstellar lines and suitable for obtaining corrections to the IUE wavelength scale. In the case of V505 Mon, only some of them can be considered as truly interstellar: namely N I, C I, Fe II and Ni II, since these lines resemble the Na D line (other lines in the list – Si II, C II, Al III – which are also referenced by Snow et al. 1994, show wide structures). The interstellar velocities are always close to zero;
- Absorption features in positions corresponding to the primary component orbital velocity appear to be present. In contrast to normal stars of similar spectral classification, these features in V505 Mon are rather

Table 4. Parameters of the binary system for various values of $q = m_1/m_2$; assumed value of inclination $i = 87°$.

q	m_1 ($M_\odot$)	m_2 ($M_\odot$)	$a_1 + a_2$ ($R_\odot$)	$R_1 + R_2$ ($R_\odot$)	$V_{\rm Kepler}{}^a$ (km s^{-1})	$V_{\rm Kepler}{}^b$ (km s^{-1})
0.5	5.1	10.2	150	13.88	−114	172
0.4	3.6	8.9	140	13.23	−113	171
0.3	2.3	7.7	130	12.28	−111	170
0.2	1.3	6.6	120	11.34	−110	169
0.15	0.9	6.0	115	10.86	−109	167
0.10	0.55	5.5	110	10.40	−108	166

[a] Calculated for phase 0.08.
[b] For phase 0.92.

narrow, probably due to the reduced carbon abundance, as discussed in Sect. 5.4;
– At phases around primary minimum, the contribution of the disk is remarkable. The rotational broadening is similar to that of the absorption component of Hα at phase 0.081. Fortunately, for the C II doublet the phase coverage is better, and the extreme velocities of the feature can be measured. Their values are discussed in Sect. 5.3.

5. Discussion

5.1. Reddening and colour indices

The reddening $E(B-V) = 0.10$ is a very low reddening for a luminous star located on the galactic equator (latitude $b = -0.°11$). In the vicinity of V505 Mon, there are members of the Mon OB2 association, with a reddening from $0\overset{\rm m}{.}4$ to $1\overset{\rm m}{.}0$, see Turner (1976). The distance of the association is 1.6 kpc. In case V505 Mon would be a true supergiant, with $M_V = -5$, its distance would be 2.5 kpc. Therefore, the low reddening is a strong argument against its supergiant nature. The HIPPARCOS parallax is rather uncertain, nevertheless, it suggests a distance larger than 500 pc. Another distance indication is the equivalent width of interstellar lines. Hobbs (1974) notes that the best correlation with distance is provided by Na I lines. In V505 Mon, the equivalent width of the interstellar component of the D_2 line is 0.25 Å. The corresponding distance is 500 pc, albeit with rather large uncertainty: judging by means of Hobbs' Fig. 7, the distance might range from 200 to 1000 pc.

The $U-B$ and $u-b$ indices during secondary eclipse are more negative than the integral light indices. In case of total eclipses, the primary component indices would equal those in secondary minimum. In case of partial eclipses, they would be yet more negative. The ultraviolet indices of the secondary component can be calculated from the integral indices, secondary eclipse indices and secondary eclipse depth; the result is $(U-B)_2 = -0.17$; then $(U-B)_1 < -0.55$ (indices 1 and 2 are used for the primary and secondary components, respectively).

5.2. Temperature and size of components

One can expect that the secondary minimum is a true eclipse of a stellar component by the primary star. In the primary minimum, however, only the sharp peak (with depth $0\overset{\rm m}{.}18$, see Table 1) in the middle of the minimum may represent the eclipse by the secondary component itself. The width of this peak is about 0.03 in phase, therefore $r_1 + r_2$ cannot be much larger than $\sin(360 \times 0.03/2) = 0.094$ (r_1, r_2 are the fractional radii of the primary and secondary components normalized to the separation of mass centers). The shapes of both minima are not well defined, nevertheless, quite strong constraints on the radii and the temperature ratio can be obtained. Since the $B-V$ and $b-y$ indices are practically identical in both eclipses and out of eclipses, the temperatures of both components should be nearly identical – as already deduced from the IUE spectra. However, the depths of both minima in V differ (if only the peak of $0\overset{\rm m}{.}18$ is considered as primary minimum), so the secondary component should be somewhat hotter. The ratio of radii cannot be determined from the existing light curve. Assuming $r_1 = r_2$ and $T_1 = 13\,000$ K, one gets $r_1 = r_2 = 0.056$, $i = 87°$ and $T_2 = 16\,500$ K. Acceptable solutions are also obtained for radii between about 0.045 and 0.067, with $r_1 + r_2 = 0.112$, and slightly different values for i and T_2.

These radii and temperatures suggest that the integral absolute magnitude M_V is in a rather narrow interval from about −2.9 to −3.2. With $V_0 = 6\overset{\rm m}{.}9$, the distance is then close to 1000 pc.

In the next section we show that the mass ratio $q = m_1/m_2$ is probably 0.3. In case of synchronous rotation, the smaller Roche lobe has a side radius of $r_{1,\rm side} = 0.272$. The observed rotational velocity is $v \sin i = 45$ km s^{-1}, which is several times faster than synchronous. Even at such velocity the Roche lobe size would still be $r_{1,\rm side} = 0.20$ (Limber 1963). Therefore, neither component is filling out its Roche lobe.

5.3. The size of the envelope and masses of components

The broad wings of the primary minimum have to be caused by an eclipse of the primary component by some sort of circumstellar matter or envelope around the secondary star. The colour independent part of the wings, as observed in bandpasses other than u or U, is probably due to electron scattering. The more pronounced shape of the wings in the UV has to be due to absorption in the Balmer continuum. The effect is larger in u than in U, since the u band is narrower and more affected by the shortest accessible wavelengths than the U band. The most probable morphology of the envelope is a disk, composed of an ionized and a neutral part. As judged from the primary minimum shape, the density of the ionized part increases in the vicinity of the secondary component; the density of the neutral part is highest not far from the outer edge of the disk.

Table 5. Rotational velocity of the disk.

Phase	0.906	0.934	0.964	0.065	0.081	0.121
Velocity ($\mathrm{km\,s^{-1}}$):						
observed	155	185	250	−150	−140[a]	−125
calculated	157	187	249	−130	−111	−81

[a] Hα.

The photometric measurements suggest that the maximum extent of both absorbing zones appears to be about equal, since in both cases attenuation of radiation occurs in the same phase interval of ±0.08 around the primary minimum. However, in a spectrum taken at phase 0.081, the effect of the disk absorption in Hα is still well noticeable. Let us take the phase limit for the disk effect as 0.085. Then $r_1 + r_{\rm disk} = \sin(360 \times 0.085) = 0.51$, i.e., after subtraction of r_1, one gets $r_{\rm disk} \approx 0.45$ or 0.46. Of course the disk has to lie inside the Roche lobe of the secondary component. Note that according to Peters (1989), the disks in Algols occupy 90 to 95% of the Roche lobe. Therefore, the Roche lobe radius $r_{\rm side}$ should be about 0.49. According to tables by Plavec & Kratochvíl (1964), the corresponding mass ratio is $q = 0.30$.

Table 4 lists parameters of the system for some values of q. In the table, a_1 and a_2 are the semiaxes of the primary and secondary orbits, R_1 and R_2 the radii of components. A particle orbiting around the secondary component in a circular orbit at a distance $a_1(1+q)\sin 2\pi\phi$ (ϕ is phase from 0 to 1) has an observable velocity (in $\mathrm{km\,s^{-1}}$)

$$V_{\rm Kepler} = V_0 + qK_1 \sin 2\pi\phi \pm 437 \sin^{-2} i \sqrt{f(m_2)(1+q)/a_1 \sin 2\pi\phi},$$

where the second term is the contribution of the secondary component velocity and the third one the circular velocity of the particle – taken positive before primary minimum, negative after ($f(m_2)$ is in units of $M_\odot$, a_1 in $R_\odot$). As one can see from the table, the observable rotational velocities of the outer disk edges do not vary much with q, and hence cannot be used to discriminate among various possible values of q.

For the value of $q = 0.30$, the velocities determined from the C II 1335/6 profile (measured at half of the absorption depth) are compared with expected rotational velocities in Table 5. The agreement with velocities calculated according to the formula is surprisingly good at the red side (before primary eclipse). At the blue side some other contribution to the profile is likely to be present, since it is impossible to explain the features marked "?" at phases 0.121, 0.169 and 0.252 as due to the disk.

With $q = 0.30$, the masses of the primary and secondary components would be 2.3 and 7.7 $M_\odot$, respectively. With these masses and radii estimated above, $\log g$ values for both components lie between 3.0 and 3.5, which agrees with values found from the fit of the IUE spectra. The parameters of the secondary are close to a main sequence star of type B3 V, the primary however appears strange. Therefore, the observed spectrum has to be a shell spectrum, the central star probably being a He star, similarly as suspected for β Lyr. The mass ratio could also be smaller; in case it should be below 0.2, the primary might be similar to the hot components of those symbiotic binaries, where a white dwarf possesses an extended atmosphere and spectroscopically resembles an A or F supergiant.

5.4. The carbon deficit

In some stars of spectral types similar to V505 Mon, the C II doublet 6578/6582 is present as a strong feature. However, in V505 Mon this doublet is entirely absent, and only C II 4267 can be suspected in several photographic spectra. Carbon lines are also absent or rather weak in the IUE spectra. Note that normally the doublet C II 1335/6 (Fig. 13) has very wide wings, which are not present in this case. The corresponding abundance amounts to only several percent of the expected value. A deficit of carbon is common in evolved stars, see, e.g. Gies & Lambert (1992).

In order to check whether the weakness of C II lines is a special feature of V505 Mon, we took spectra around Hα of several other B-type stars (with the Reticon attached to the coudé spectrograph of the 2 m telescope in Ondřejov). The equivalent widths are listed in Table 6, and can be compared with theoretical values (Kubát 1996) in Table 7.

The C II 6578/6582 doublet is obviously absent or weak in several cases. Very strong underabundance of carbon was found in β Lyr by Balanchandran et al. (1986) – no doubts that this is due to the mass transfer in the system. Yet one cannot conclude that mass transfer is always responsible for the carbon deficit. In the case of V505 Mon, mass transfer must however have played an important role, because the orbit must have been circularized by this process. Usually binaries with similar parameters have eccentric orbits, since due to the long period and small sizes of components, tidal effects alone would not be sufficient as a circularization mechanism.

5.5. The cloudy nature of the circumstellar matter

The photometric variability and the changes of line profiles suggest that the disk is strongly variable. It is also evident that clouds of various velocities exist; since irregular velocities appear for lines of very different excitation, the clouds should also differ in their temperature.

The brightness decreases observed at out-of-eclipse phases are enhanced in u (or U), i.e. the processes responsible should be comparable to those causing the effects observed in the wings of the primary minimum: the clouds should be composed of neutral and ionized parts. Attenuation of light by circumstellar clouds has also been documented in the case of AX Mon (Elias et al. 1997), and has generally been treated by Wilson (1999). Note that absorption in Hα and profiles of He and Na lines at phases around 0.8 in AX Mon are very similar to those of

Table 6. C II and He I equivalent widths (EW, in mÅ) for various B-type stars.

Spectral type	Luminosity class	HD number	Binary comp.	EW[a] C II 6578	EW C II 6582	EW He I 6678
B1	Ib	91316		142	118	961
	III	23180	pri	n[b]	n	649
	V	116658	pri	n	n	655
B2	III	35468		288	221	744
B3	III	116658	sec	n	n	144
	III	174237		n	n	321
	III	25204	pri	120	98	459
B5	Iab	36371		380	296	887
	Ib	48914		n	n	827
	Ib	164353		379	289	729
B6	III	155763		n	n	156
	V	23338		n	n	170
B7	III	35497		n	n	116
	V	139892	pri	n	n	65
B9	Ia	34085		214	170	528

[a] In case of binaries, EWs refer to the composite continuum of both binary components.
[b] n – line is not observed.

Table 7. Theoretical equivalent widths of C II lines (in mÅ).

$T_{\rm eff}$[K]	19 000	16 000	13 000	19 000	16 000	13 000	19 000	16 000	13 000	19 000	16 000	13 000
Line	$\log g = 3.0$			$\log g = 3.5$			$\log g = 4.0$			$\log g = 4.5$		
4267.1[a]	–	–	234	–	–	212	974	252	–	–	–	–
6578.1	320	239	180	379	238	162	428	189	130	401	188	117
6582.9	238	209	159	268	195	138	303	170	106	219	165	80

[a] Sum of values for 4267.000 and 4267.260 is given.

V505 Mon at phase zero. Various absorption components in Hα – probably due to clouds – were also observed in Algol (Richards 1993).

5.6. Comparable stars

For comparison, we will discuss some emission-line binaries – albeit non-eclipsing ones – which are of similar structure and exhibit related effects like V505 Mon.

V742 Cas (HD 698; Hutchings & Bernard 1978; Sahade 1967; Sahade et al. 1992) is certainly such a case. The period of 56 days and its classification as B7 II/Ib are nearly identical with the V505 Mon values, and in its photographic spectra only lines of the primary component are visible (with $K = 87.5$ km s^{-1}). There is a similarity in the photometric behaviour as well: according to the HIPPARCOS photometry, V742 Cas is variable on a short time scale, see Fig. 14. Also Hα emission behaves similarly as in V505 Mon; concerning V742 Cas, Sahade writes: "The fact that ... the Hα velocities do not seem to vary with phase and fall below the γ-velocity strongly suggest that the emission arises in a circumbinary envelope." Sahade et al. (1992) studied two IUE spectra and found several sets of lines of various widths, radial velocities and excitation, and give $v_{\rm rot} \sin i \approx 80$ km s^{-1}.

The binary V447 Sct (HD 173219) is of earlier type – B0/1 Ve, according to Hiltner (1956). The star was studied by Hutchings & Redman (1973). They note that strong spectral features indicate a type B2 Ib; and that the spectrum partly arises in a shell or extended envelope. Also in this case some parameters are very similar to V505 Mon: the period is 58 days, only the primary component lines are visible, with a semiamplitude of 94 km s^{-1} (which, however, differs for various ions). The radial velocity curve is poorly defined, therefore a circular orbit is possible in spite of a discordant eccentricity value of $e = 0.16$ given by Hutchings & Redman. Photometry was obtained in the LTPV program, and was discussed by Sterken et al. (1996). The star was measured also by

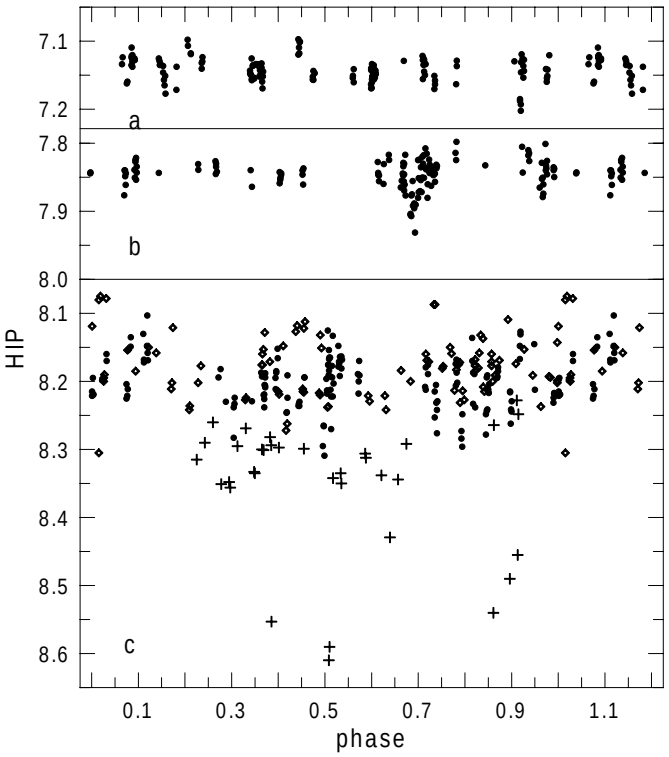

Fig. 14. Photometric behaviour of binaries similar to V505 Mon (phase is zero for the conjunction corresponding to a primary minimum; filled circless: HIPPARCOS) **a)** V742 Cas (HD 698), 2443328.671 + $55\overset{\mathrm{d}}{.}9233\cdot$ E (Sahade et al. 1992) **b)** V447 Sct (HD 173219), 2438965.8+$58\overset{\mathrm{d}}{.}395\cdot$ E (Hutchings & Redman 1973) **c)** V1362 Cyg (HD 190467), 2429821+$56\overset{\mathrm{d}}{.}76\cdot$ E (this paper); crosses: Percy (1970), open squares: Hill et al. (1976).

HIPPARCOS; the brightness is again somewhat variable (Fig. 14).

Another similar case is HD 190467, type B6 Ib. Percy (1970) discovered its variability, and the star has been named V1362 Cyg. Photometric measurements were also made by Hill et al. (1976), and HIPPARCOS photometry is available, too (Fig. 14). Ten published radial velocities (Petrie & Pearce 1961, Abt 1973) are compatible with a period of $56\overset{\mathrm{d}}{.}76$, $K = 65$ km s^{-1}. Based on additional data, Hill et al. note that no other period than ≈57 days is possible (and they consider the star as "a very interesting, if enigmatic object"). No spectroscopic study has been done for this star (and no IUE spectra exist). According to Henize (1976) the Hα emission is modest/weak.

It appears that no phase dependent photometric features are present in any of these cases.

5.7. Conclusions

It seems that there is no other eclipsing early-type binary comparable to V505 Mon, with such well manifested presence of various forms of circumstellar matter. However, similar systems exist. Very probably, in V505 Mon and all other binaries mentioned the supergiant appearance is only simulated. Discussing normal Be stars, Harmanec (1983, 2000) speaks about a pseudophotosphere, meaning the inner, densest layer of the envelope close to the star. Therefore, besides the disk around the secondary star and an extended circumbinary envelope, there is probably also an envelope surrounding the primary star.

Believing that the circular orbit of V505 Mon is due to mass transfer and that the mass ratio is small, the system has to be a result of case B evolution. Only a speculative model of the binary can be offered: the primary component – the remnant of the originally more massive star, now probably a He star – provides some steady outflow of matter needed to feed the circumbinary matter and to produce a stationary situation. Note that such an outflow has been assumed, e.g. in case of ϕ Per (Gies 2000).

Many important questions remain to be answered. Besides the parameters of components, it is mainly the reason of invisibility of the secondary lines and the source of the circumstellar matter, which is still to be clarified. However, these questions have also not been answered adequately for several other interacting binaries with undersized components.

Acknowledgements. The authors are indebted to Dr. Kubát for calculations of C II equivalent widths. The late Dr. Popper kindly allowed us to use his spectra (Lick 3 and 4). Drs. G. Hill and Wenxian Lu participated in obtaining and analysing the DAO spectra. Referee Dr. Bakker suggested valuable changes to the manuscript. The IUE spectra were transferred from the NASA IUE archive. Dr. Chochol's participation was enabled by the VEGA grant 1157.

References

Abt, H. A. 1973, ApJS, 26, 365
Balanchandran, S., Lambert, D. L., Tomkin, J., & Parthasarathy, M. 1986, MNRAS, 219, 479
Batten, A. H., Fletcher, J. M., & MacCarthy, D. G. 1989, Publ. DAO Victoria, 17, 1
Chochol, D. 1981, Publ. Astr. Inst. Czechosl. Acad. of Sci., 57, 30
Chochol, D., & Kučera, A. 1981, IBVS, 1998
Chochol, D., Bakos, G. A., Bartolini, C., et al. 1985, Contr. Skalnate Pleso, 13, 75
Chochol, D., et al. 2001, Contr. Skalnate Pleso, in preparation
Eggen, O. C. 1978, AJ, 83, 288
Elias, N. M., Wilson, R. E., Olson, E. C., et al. 1997, ApJ, 484, 394
ESA 1986, IRAS Catalogue, Noordwijk, ESA
ESA 1997, The Hipparcos and Tycho Catalogues, ESA SP-1200, Noordwijk, ESA
Gies, D. R. 2000, in The Be Phenomenon in Early-Type Stars, ed. M. A. Smith, H. F. Henrichs, & J. Fabregat, 668
Gies, D. R., & Lambert, D. L. 1992, ApJ, 387, 673
Harmanec, P. 1983, Hvar Obs. Bull., 7, 55
Harmanec, P. 2000, in The Be Phenomenon in Early-Type Stars, ed. M. A. Smith, H. F. Henrichs, & J. Fabregat, 13
Henize, K. G. 1976, ApJS, 30, 491
Hill, G., Hilditch, R. W., & Pfannenschmidt, E. L. 1976, Publ. DAO Victoria, 15, 1

Hiltner, W. A. 1956, ApJS, 2, 313
Hoag, A. A., & Smith, E. v. P. 1959, PASP, 71, 32
Hobbs, L. M. 1974, ApJ, 191, 381
Hutchings, J. B., & Bernard, J. E. 1978, PASP, 90, 179
Hutchings, J. B., & Redman, R. O. 1973, MNRAS, 163, 219
Kubát, J. 1996, private communication
Kurucz, R. L. 1993, CD ROM, No. 13
Limber, D. N. 1963, ApJ, 138, 1112
Manfroid, J., Sterken, C., Bruch, A., et al. 1991, ESO SR, No. 8
Manfroid, J., Sterken, C., Cunow, B., et al. 1994, ESO SR, No. 14
Olson, E. C., & Etzel, P. B. 1995, AJ, 109, 1308
Pearce, J. A., & Petrie, R. M. 1951, Publ. DAO Victoria, 8, 409
Percy, J. R. 1970, J. R. Astron. Soc. Can., 64, 218
Peters, G. J. 1989, Space Sci. Rev., 50, 9
Petrie, R. M., & Pearce, J. A. 1961, Publ. DAO Victoria, 12, 1
Plavec, M., & Kratochvíl, P. 1964, Bull. Astr. Inst. Czechoslovakia, 15, 165
Richards, M. T. 1993, ApJS, 86, 255
Sahade, J. 1967, in Modern Astrophysics, ed. M. Hack (Gauthier-Villars, Paris), 219
Sahade, J., Barbá, R., & Kondo, J. 1992, ApJS, 81, 303
Snow, T. P., Lamers, H. J. G. L. M., Lindholm, D. M., & Odell, A. P. 1994, ApJS, 95, 163
Stagni, R., Margoni, R., & Mammano, A. 1982, Ap&SS, 88, 115
Sterken, C., Manfroid, J., Anton, K., et al. 1993, ESO SR, No. 12
Sterken, C., Manfroid, J., Beele, D., et al. 1995, ESO SR, No. 16
Sterken, C., Vogt, N., & Mennickent, R. E. 1996, A&A, 311, 579
Stickland, D. J. 1987, Observatory, 107, 5
Turner, D. G. 1976, ApJ, 210, 65
Vogt, N., & Sterken, C. 1993, IBVS, 3958
Wachmann, A. A. 1966, Astr. Abh. Hamburg-Bergedorf, 7, 341
Wilson, R. E. 1999, in Modern Astrometry and Astrodynamics, ed. R. Dvorak, F. H. Haupt, & K. Wodnar (Wien), 219